

Supplemental Data

Germline and Mosaic Variants in *PRKACA* and *PRKACB*

Cause a Multiple Congenital Malformation Syndrome

Adrian Palencia-Campos, Phillip C. Aoto, Erik M.F. Machal, Ana Rivera-Barahona, Patricia Soto-Bielicka, Daniela Bertinetti, Blaine Baker, Lily Vu, Francesca Picci-Sparascio, Isabella Torrente, Eveline Boudin, Silke Peeters, Wim Van Hul, Celine Huber, Dominique Bonneau, Michael S. Hildebrand, Matthew Coleman, Melanie Bahlo, Mark F. Bennett, Amy L. Schneider, Ingrid E. Scheffer, Maria Kibæk, Britta S. Kristiansen, Mahmoud Y. Issa, Mennat I. Mehrez, Samira Ismail, Jair Tenorio, Gaoyang Li, Bjørn Steen Skålhegg, Ghada A. Otaify, Samia Temtamy, Mona Aglan, Aia E. Jønch, Alessandro De Luca, Geert Mortier, Valérie Cormier-Daire, Alban Ziegler, Mathew Wallis, Pablo Lapunzina, Friedrich W. Herberg, Susan S. Taylor, and Victor L. Ruiz-Perez

Supplemental Case Reports

Family 1. The proband is a 33-year-old Egyptian male who presented with postaxial polydactyly and history of two previous offspring deaths from a non-consanguineous marriage, both had short limbs, postaxial polydactyly and congenital heart disease.

The first pregnancy was a boy delivered at full term by caesarean section (CS). This baby had postaxial polydactyly in both hands, short limbs, nail dystrophy and congenital heart defect. Respiratory distress and meconium aspiration at birth needed incubation and mechanical ventilation. The boy died at 17 days from respiratory failure. The second pregnancy was a girl born at full term by CS. She had the same manifestations of her brother and was incubated for 4 days. Echocardiography at 4 months of age revealed atrioventricular canal (AVC) with common atrium, atrial septal defect measuring 2 cm. The left atrium was relatively small with small mitral valve annulus. There was subaortic ventricular septal defect (VSD) measuring 0.25 cm with no apparent flow because of severe pulmonary hypertension (PHTN). There was prolapse of anterior mitral leaflet with subsequent mitral regurgitation (MR III) and peak velocity 3.5 m/sec and she died at 4.5 months from cardiac and respiratory failure.

Examination of the proband revealed a stocky body built, relatively long trunk and generalized hirsutism. He has long face with mid face hypoplasia, prominent nose, overhanging nasal tip, short philtrum and short neck. Orofacial assessment revealed asymmetry of face, hypoplastic maxilla, short lingual frenum, multiple upper and lower lingual frenula, diastema, crossbite, congenitally missing upper lateral incisors, bilateral, and lower right lateral incisor. His height was 165 cm (- 1.61 SD) with arm span of 162.2 cm, weight was 97 kg (+ 1.74 SD) and head circumference of 57 cm (+ 1.32 SD). Examination of limbs showed postaxial polydactyly of both hands and feet (surgical removal of the extra digit was performed on the right hand and foot) and wide space between big toe and second toe in both feet. His nails were normal. Echocardiography was done for screening and it was normal. His wife was normal at time of first presentation to the clinic.

Abdominal ultrasound (US) conducted in the proband at age 33 years was found normal apart from fatty liver. No suprarenal abnormalities were detected by US. The following endocrinology lab tests were also performed at the same age (reference values are indicated between brackets): serum calcium: 9.5 mg/dL (8.5-10.2), serum phosphorous: 4 mg/dL (2.5-4.5), TSH: 4.65 uIU/mL (0.55-4.78), FT4: 1.2 ng/dL (0.8-1.8), Prolactin: 20.4 ng/mL (4-15.2), Testosterone-total: 2.86 ng/mL (2.6-10), Cortisol – am: 10.53 ug/dL (6.2-19.4), ACTH –am: 20.15pg/mL (7.2-63.3), Growth hormone

(basal): 0.03 ng/mL (0.03-2.47), insulin like growth factor 1 (IGF1): 173 ng/mL (43-209), Parathyroid hormone (PTH): 63 pg/mL (15-65), and 25 OH vitamin D: 10.32 ng/mL (deficient <20). All lab results were normal except prolactin that was mildly elevated and vitamin D low. However, this man does not have any manifestations of hyperprolactinemia (no headache, no gynecomastia, no fertility problems, normal testosterone, normal liver and kidney functions) and by history he did not receive any medications for hypertension, gastroesophageal reflux, nausea, vomiting, depression or antipsychotics that may elevate prolactin levels. Hyperprolactinemia is usually defined as fasting levels of above 20 ng/mL in men and above 25 ng/mL in women. Prolactinoma is likely if prolactin levels are greater than 250 ng/mL. Follow up was scheduled to ensure whether this is persistent hyperprolactinemia or a transient event. He had low 25 OH vitamin D, but serum calcium and PTH were normal. He has started oral treatment with vitamin D3.

After examination of the proband, the couple had a third pregnancy that resulted in an affected girl with similar clinical manifestations as the previous siblings. This girl died intrauterine at 33 weeks of gestation due to wrapped cord around the neck with true knot of the cord. She was delivered by CS and the skin was macerated. Another following pregnancy was terminated at 16 weeks of gestation because of a similarly affected fetus with congenital heart disease in the form of single ventricle and abnormalities of great vessels, short long bones and postaxial polydactyly. Samples were taken from both fetuses for molecular studies.

Family 2. The proband is a 42-year-old female born to non-consanguineous and healthy parents of Belgian origin. She was born at term with a birth weight of 3100 g, length of 46 cm and head circumference of 34 cm. She presented after birth with postaxial hexadactyly of both hands, narrow thorax, short limbs and nail dysplasia on fingers and toes. Multiple oral frenula were also visible in the mouth. At the age of 2 months she underwent a lobectomy because of emphysema in the upper lobe of the left lung. At 20 months of age the extra fingers were surgically removed. Clinical evaluation at the age of 35 years revealed disproportionate short stature with a height of 139 cm (- 5 SD) and an arm span of 121 cm. She had short limbs with significant brachydactyly of hands and feet and nail dysplasia on fingers and toes. Her weight was 61.5 kg (+ 0.46 SD) and head circumference was 52.6 cm (- 1.6 SD). The thorax was not narrow. She had bilateral cubitus valgus and genua valga. In the mouth, no frenula were found. She had multiple dental crowns. She gave birth to two healthy sons. The second pregnancy resulted in a miscarriage. The third pregnancy was terminated at 24 weeks. Ultrasound evaluation of the female fetus revealed short limbs, narrow thorax,

congenital heart defect and postaxial polydactyly on both hands. Postmortem examination confirmed the presence of short limbs, postaxial hexadactyly of both hands, short ribs and complete atrioventricular septal defect of the heart.

Recent endocrine investigations in this proband showed test values within the normal range. Serum calcium: 2.40 mmol/L (2.18-2.60), serum phosphate: 1.19 mmol/L (0.78-1.65), calcium phosphate: 3.0 mmol²/L² (<4.0), TSH: 1.20 mU/L (0.55-4.78), FT4 free: 16.4 pmol/L (11.5-22.7), Prolactin: 8.2 µg/L (2.8-29.2), Growth hormone: 2.6µg/L, IGF1: 181ng/mL (76-234), PTH (1-84): 26 ng/L (18.5-88.0), 25-OH vitamin D: 27ng/mL (9-48), ACTH: 22 pg/mL (7-63), cortisol –am: 105.0 ng/mL. Ultrasound of kidneys and suprarenal glands revealed no abnormalities.

Family 3. The proband was a female fetus suspected of having Ellis-van Creveld syndrome based on ultrasonographic imaging findings. She was the first pregnancy of healthy non-consanguineous parents of Italian origin. Due to fetal anomalies, the pregnancy was terminated at 23 weeks of gestation and a fetal autopsy was performed. Fetus length and weight were 27 cm (<3%) and 467 g (25%<p<50%), respectively. Radiological evaluation revealed micromelia, short ribs and narrow thorax. Examination of limbs showed postaxial hexadactyly of both hands and of the left foot. Echocardiography highlighted the presence of atrioventricular canal defect with myocardial hypertrophy. Histological assessment pointed out both lungs with immature parenchyma at canalicular stage, meanwhile renal, hepatic and pancreatic parenchyma were normal, thus excluding hepato-renal-pancreatic dysplasia. Moreover, the fetus presented with cerebral edema and genitourinary malformation, specifically, a bicornuate and didelphys uterus was observed. Given the earliness of the observation, the possible ectodermal dysplasia could not be evaluated. The family had a second son. He was born healthy, and referred healthy at 2 years of age.

Family 4. Proband 4 is an 18-year-old female, the 2nd child of healthy non-consanguineous parents. She was born at 40 weeks and 2 days of gestation with a birth weight of 3660 g, birth length 54 cm, and head circumference 35 cm. She was born with bilateral postaxial polydactyly of hands and feet, that was surgically corrected at 9 months of age. At the time of surgery, a congenital heart defect was detected due to a low oxygen saturation (90%) and arrhythmias. Echocardiogram showed partial AVSD (ASD type 1 ostium primum defect) and left cava superior entering into the coronary sinus, considered a rare anatomic variant that was surgically corrected at the age of 14 months. After successful heart surgery she had, as expected, a slight mitral valve insufficiency, without hemodynamic importance, notable as a grade 1 systolic

murmur at the left sternal border/apex. At the age of six years, she had hip surgery performed due to coxa vara (bilateral intertrochanteric osteotomy).

This girl is generally healthy. She had a single episode of febrile seizure at the age of two years. At the age of 12 years she needed glasses to correct for myopia. Her hearing is normal. General physical examination revealed mild disproportionate short stature with shortening of both upper and lower limbs. She is currently 163 cm (- 1 SD), weight 47.3 kg (- 2.8 SD) and has a head circumference of 51 cm (- 3 SD). Parental heights are 176.3 cm and 176.1 cm, respectively. She presents a long and narrow thorax, bilateral genu valga and mild cubitus varus. Hands and feet are short and broad with shortening of middle and distal phalanges and toes (current shoe size 35). Further broadening of distal phalanges 2 to 5, and first fingers and toes are noted. The girl is only able to hold a pencil for a short period of time.

Nails are dysplastic especially on the toes, and broad on first finger bilaterally. The hair was fine but not sparse. Mild facial dysmorphism including a long facial appearance and neck, a broad chin and nose as well as a short and deep philtrum was noticed. The upper lip is tented and nasolabial folds are underdeveloped. Ears are low set and small with small lobes and prominent superior crus. Intraoral examination revealed small maxillary central incisors and a conical right canine, as well as hypodontia, invagination, agenesis and supernumerary teeth of mandibular lateral incisors. Oral frenula are not present, but fusion of parts of the upper and lower lip to the maxillary and mandibular gingival mucosa was noted. She is currently wearing bracelets on upper and lower teeth as part of her dental care.

A developmental evaluation, which took place when the girl was approximately 4 ½ years, revealed mild language delay, gross motor difficulties and balance problems as well as concentration problems and a developmental level of 3 to 3.9 years using the Psychoeducational Profile Revised (PEP-R) and the Wechsler Preschool and Primary Scale of Intelligence-Revised (WPPSI-R), respectively. To improve development, she received physiotherapy and part-time pedagogical support as well as exercise at home. She went through an ordinary school program, and she now attends an ordinary high school program. She was diagnosed with dyslexia at the age of 11 years, and she used a special computer developed for dyslexic individuals for her schoolwork. Due to later unremarkable development no formal cognitive assessments have been carried out at older age.

X-ray of hands and feet before surgical removal of the extra-digits at the age of 9 months had shown a 6th rudimentary finger bilaterally with rudimentary metacarpal

bones and proximal phalanges. Middle and distal phalanges were not visible. In addition, the right 5th metacarpal bone was irregular and broad. Bilateral complete 6th toes with presence of metatarsal bones and phalanges were also observed. X-ray of hands and feet was repeated at age three years. Right hand showed some signs of the previously surgically corrected polydactyly on the 5th metacarpal bone. All metacarpal bones were short and slightly plumb. The middle phalanges were short and wide with “bell shaped” epiphyses and hypoplasia of distal phalanges was also present. The shape and size of the proximal phalanges were normal. Both feet were broad with short metatarsal bones. Anteroposterior (AP) X-ray view of upper and lower limbs, also at the age of three, showed the length of ulna, radius, and the long bones of the lower limbs (femur, tibia and fibula) mildly shortened. The clinical findings were suggestive of Ellis-van Creveld syndrome and she was seen regularly during childhood at the Departments of Orthopedics, Pediatrics and Cardiology as well as the Dentist.

Endocrine investigations performed at current age showed serum levels of hormones generally normal. Cortisol–am (8:30 am): 433 nmol/L (reference 200-700), ACTH: 2.5 pmol/L (1.6-14), PTH: 5.7 pmol/L (1.6-6.0), somatotropin (GH): 0.81 µg/L, IGF1: 381 µg/L (149-459) and TSH: 1.2 mIU/L (0.50-4.3). Serum levels of calcium: 1.25 mmol/L (1.18-1.32), phosphate: 1.33 mmol/L (0.76-1.41) and 25-hydroxy vitamin D: 64 nmol/L (50-160) were also normal. Recent abdominal MRI scan of this proband revealed no adrenal lesions.

Family 5. The proband is a girl, first child of healthy parents. She was born at 39 weeks with a birth weight of 2600 g, birth length 48 cm and head circumference 35 cm. She presented with bilateral postaxial polydactyly of both hands and multiple oral frenula. Echocardiogram detected an atrioventricular septal defect with single atrium and mitral anomaly and she had open-heart surgery to repair. She had a long and narrow thorax and abnormal teeth (hypodontia). She had a normal development. At 14 years of age, her height was at 148.5 cm (- 1.8 SD) and weight 41 Kg (- 1 SD). The girl presented a long and narrow thorax and bilateral genu valgus. Hands and feet were short and broad with shortening of middle and distal phalanges of toes (shoe size 33). She had also some degree of hyperlaxity.

Family 6. Proband 6 is a male, the third child of an unrelated couple of French origin. The family history is remarkable for a single atrium in a paternal cousin of the proband. He was born with a single atrium and postaxial polydactyly of all four limbs requiring surgery. Following this surgery, he developed localized myoclonus (upper limb) consecutive to an ischemic stroke. These seizures were efficiently treated with

carbamazepine until the age of two years. MRI brain performed at one year of age for this stroke did not reveal any associated malformations.

Independent walking was acquired at the age of 30 months. Growth is normal (at 20 years: height 175 cm (M), weight 53 kg (- 1.5 SD) and OFC 56.5 cm (+ 0.5SD)). The acquisition of speech has been slightly delayed. At the last examination, he was perfectly able to communicate despite a fluctuating stuttering. A specialized education has enabled the boy to acquire reading and writing. He was autonomous (living in his own apartment and working as an Interim employee). Routine abdominal ultrasound at age 20 years was normal.

Family 7. The proband is a 41-year-old female born to a non-consanguineous Australian/Caucasian couple where the pregnancy was complicated by premature labour and vaginal bleeding at six months gestation, which spontaneously stopped. She was born with a single umbilical artery at term, with a birth weight of 3500 g and head circumference of 34.5 cm, in poor condition, which improved quickly and she was discharged from hospital a few days later. Postaxial polydactyly of both feet and right hand was noted after birth, and these extra digits were surgically removed in later childhood. After a period of poor feeding in infancy, she re-presented to hospital at five weeks with cyanotic heart disease requiring open-heart surgery to repair a complete atrioventricular septal defect with common atrium. She had persistent pneumonia and cardiac failure post-surgery and was discharged at 3 months of age. Developmentally, she smiled at 3-4 months of age, rolled at 13 months of age, laughed at 15 months and walked at five years of age with assistance after developmental regression at two years of age with loss of speech. An early pelvic X-ray showed prominent iliac wings with a notch below the sacroiliac joints (films not available for review). She had refractory focal epilepsy with onset of focal impaired awareness seizures (FIAS) at eight years of age and developed aggressive behaviour at 9 years. She had a single episode of nonconvulsive status epilepticus (NCSE) at ten years of age and also has nocturnal tonic seizures. In adulthood, she has severe intellectual disability with limited mobility, autistic features and mild generalised spasticity. She has a history of multiple several tumors including a grade 1 borderline mucinous ovarian tumour at 17 years, liver haemangioma, and a renal cell carcinoma at 17 years. Other history includes hyperprolactinaemia attributed to haloperidol use for aggression, deformed tympanic membranes with good hearing, atrial fibrillation with persistent valvular incompetence, osteoporosis with multiple fractures resulting in her being unable to weight-bear or walk from 38 years, dural ectasia, recurrent dislocated patellae, and gastroesophageal reflux disease.

On examination in adulthood, she had an asthenic build and normal stature. Facially, she had a broad forehead, hypertelorism, prognathism, and a prominent nasal tip and an asymmetric nasal bridge related to a prior fracture. There was no obvious midline cleft of her lip or tongue, or accessory oral frenula. Her ear morphology and position looked normal. She had broad toes, mild digital clubbing, fifth finger clinodactyly, and scars on her feet and right hand from previous polydactyly surgery.

Her investigations included MR brain that documented asymmetric brachycephaly with a prominent pituitary, and an EEG showed right centro-parietal slowing. Bone densitometry revealed low for age bone mineral density with a lowest T-score of -2.6 in AP spine. Her serum corrected calcium (2.35 mmol/L (2.15-2.65)) and her phosphate (1.2 mmol/L (0.8-1.4)) levels were normal. She also had normal serum 25-hydroxy vitamin D (126 nmol/L (>50)). Her serum prolactin was elevated at 942 mIU/L (59-619) and she has had slightly low thyroid stimulating hormone (TSH; 0.32 mIU/L (0.50-4.00)) with normal free thyroxine (FT4; 15.5 pmol/L (10.0-19.0)). She had no adrenal lesions reported on abdominal CT or ultrasound imaging.

Supplemental Figures

Figure S1

PRKACA (p.Gly137Arg)			PRKACB (p.Ser54Leu)		
<i>Hs</i>	EMFSLRRIGRFSEPHARF	NP_002721.1	<i>Hs</i>	ERKKTLTGTSFGRVMLVKH	NP_002722.1
<i>Mm</i>	EMFSLRRIGRFSEPHARF	NP_032880.1	<i>Mm</i>	ERKKTLTGTSFGRVMLVKH	NP_035230.1
<i>Xl</i>	EMFSLRRIGRFSEPHARF	NP_001093339.1	<i>Xl</i>	DRMKTLTGTSFGRVMLVKH	NP_001080696.1
<i>Dr</i>	EMFSLRRIGRFSEPHARF	NP_001076309.1	<i>Dr</i>	DRQKTLTGTSFGRVLLVKH	NP_001030148.1
<i>Dm</i>	EMFSLRKRGRFSEPHSRF	NP_476977.1	<i>Dm</i>	ERIKTLTGTSFGRVMIVQH	NP_476977.1
<i>Ce</i>	EMFSLRRIGRFSEPHSRF	NP_001350982.1	<i>Ce</i>	DRIKTLTGTSFGRVMLVKH	NP_001350982.1
<i>Ac</i>	EMFSLRRIGRFSEPHSRF	NP_001191420.1	<i>Ac</i>	DRIKTLTGTSFGRVMLVQH	NP_001191420.1
PRKACB (p.His88Arg and p.His88Asn)			PRKACB (p.Gly235Arg)		
<i>Hs</i>	KVVKLKQIEHTLNEKRILQ	NP_002722.1	<i>Hs</i>	GVLİYEMAAGYPPFFADQP	NP_002722.1
<i>Mm</i>	KVVKLKQIEHTLNEKRILQ	NP_035230.1	<i>Mm</i>	GVLİYEMAAGYPPFFADQP	NP_035230.1
<i>Xl</i>	KVVKLKQIEHTLNEKRILQ	NP_001080696.1	<i>Xl</i>	GVLİYEMAAGYPPFFADQP	NP_001080696.1
<i>Dr</i>	KVVKLKQVEHTLNEKRILQ	NP_001030148.1	<i>Dr</i>	GVLİYEMAAGYPPFFADQP	NP_001030148.1
<i>Dm</i>	KVVKLKQVEHTLNEKRILQ	NP_476977.1	<i>Dm</i>	GVLİYEMAAGYPPFFADQP	NP_476977.1
<i>Ce</i>	KVVKLKQVEHTLNEKRILQ	NP_001350982.1	<i>Ce</i>	GVLİYEMAAGYPPFFADQP	NP_001350982.1
<i>Ac</i>	KVVKLKQVEHTLNEKKILQ	NP_001191420.1	<i>Ac</i>	GVLİYEMAAGYPPFFADQP	NP_001191420.1

Figure S1. C α and C β mutated residues are evolutionarily conserved. Each panel shows a stretch of amino acids from human C α (*PRKACA*) or C β (*PRKACB*) comprising the mutated residues found in affected individuals (red letters) aligned to the corresponding sequences of C α and C β PKA subunits from different vertebrates. The sequences of homologous cAMP-dependent protein kinase catalytic subunits from three invertebrates are also shown. *Homo sapiens* (*Hs*), *Mus musculus* (*Mm*), *Xenopus laevis* (*Xl*), *Danio rerio* (*Dr*), *Drosophila melanogaster* (*Dm*), *Caenorhabditis elegans* (*Ce*), *Aplysia californica* (*Ac*). Residues that are non-identical to the human proteins are in black letters. Protein reference numbers are indicated.

Figure S2. WES Results and Analysis Pipelines

Individual 1

total number of single nucleotide variations (SNVs)	MAF (gnomAD v2.1.1. liftOver hg38) ≤ 0.001	loss-of function variants or missense	CADD PHRED score >20 and polyphen2 predicted damaging	Present in affected daughter (II-3)	Genes in common with WES results from individual 2
143223	12262	719	194	69	1

Individual 2

Total number of SNVs	variants present in affected foetus (III-3)	MAF gnomAD ≤ 0.001	Coding nonsynonymous variants, indels or splicing variants	CADDv1.4 >20 and Polyphen2 predicted damaging	Genes in common with WES results from individual 1
58483	23709	472	118	40	1

Comparison of WES results between families 1 and 2 with very similar phenotypes identified only one gene in common: *PRKACA*. All affected individuals from both families carried the same *PRKACA* variant NM_002730.4: c.409G>A (p.Gly137Arg). Individual 1 was also heterozygous (VAF:0.49) for a missense variant of uncertain significance in *GPR161*: NM_001267609.1: c.263G>A (p.Ser88Asn) that was among the 69 variants present in his affected daughter (II-3 in Figure 1A). Heterozygous variants in *GPR161* have been associated with risk of spina bifida¹ and in a consanguineous family, a recessive missense variant in *GPR161* was associated with Pituitary Stalk Interruption Syndrome².

Individual 4

Total number of SNV	Variants with allele frequency $< 1\%$ in ALL population from the phase III of the 1000 Genomes Project	Coding nonsynonymous variants, indels or splicing variants	Variants classed as deleterious at least by half of four pathogenicity predictors (SIFT, Polyphen, Mutation Taster, CADD)	Recessive model	<i>De novo</i>
358133	41152	1382	794	92	6

Manual inspection identified the *PRKACB* (NM_002731.3) *de novo* variant c.703G>C (p.Gly235Arg) as the likely cause of the disease. The rest of variants were overrepresented in control population databases (dbSNP) or corresponded to polymorphic indel positions.

Individual 5

Total number of SNV	Variants with allele frequency < 1% in dbSNP, 1000 genomes, Exome Variant Server, Exac, gnomAD	Coding nonsynonymous variants, indels or splicing variants	Variants in neither "In-House" exomes	Variants considered by SIFT or Polyphen as surely damaging and CADD score >30
122765	18718	4950	90	3

Selected variant: *PRKACB*: c.161C>T (p.Ser54Leu). Other WES findings of uncertain significance: *USP40*: c.1586G>A (p.Arg529Lys); *ADAD2*: c.1795C>T (p.Arg599Cys).

Individual 6

Total number of SNVs	MAF gnomAD ≤ 0.01%	Removing intergenic or non-coding variant	CADD≥20 and damaging by Polyphen or SIFT	Inheritance mode and BAM validation
45812	3831	993	130	1

Selected variant: *PRKACB*: c.263A>G (p.His88Arg)

Individual 7

Total number of SNVs	Exonic or splicing	Remove synonymous SNVs	Filter gnomAD allele frequency	Filter inheritance model	Manually inspected
495726	36200	22392	1321	60	3 (one proven to be a sequence artefact by Sanger sequencing validation)

Selected variant: *PRKACB*: c.262C>A (p.His88Asn). Other WES findings of uncertain significance: *PIGR*: c.155G>A (p.Arg52Gln (*de novo*)).

Figure S3

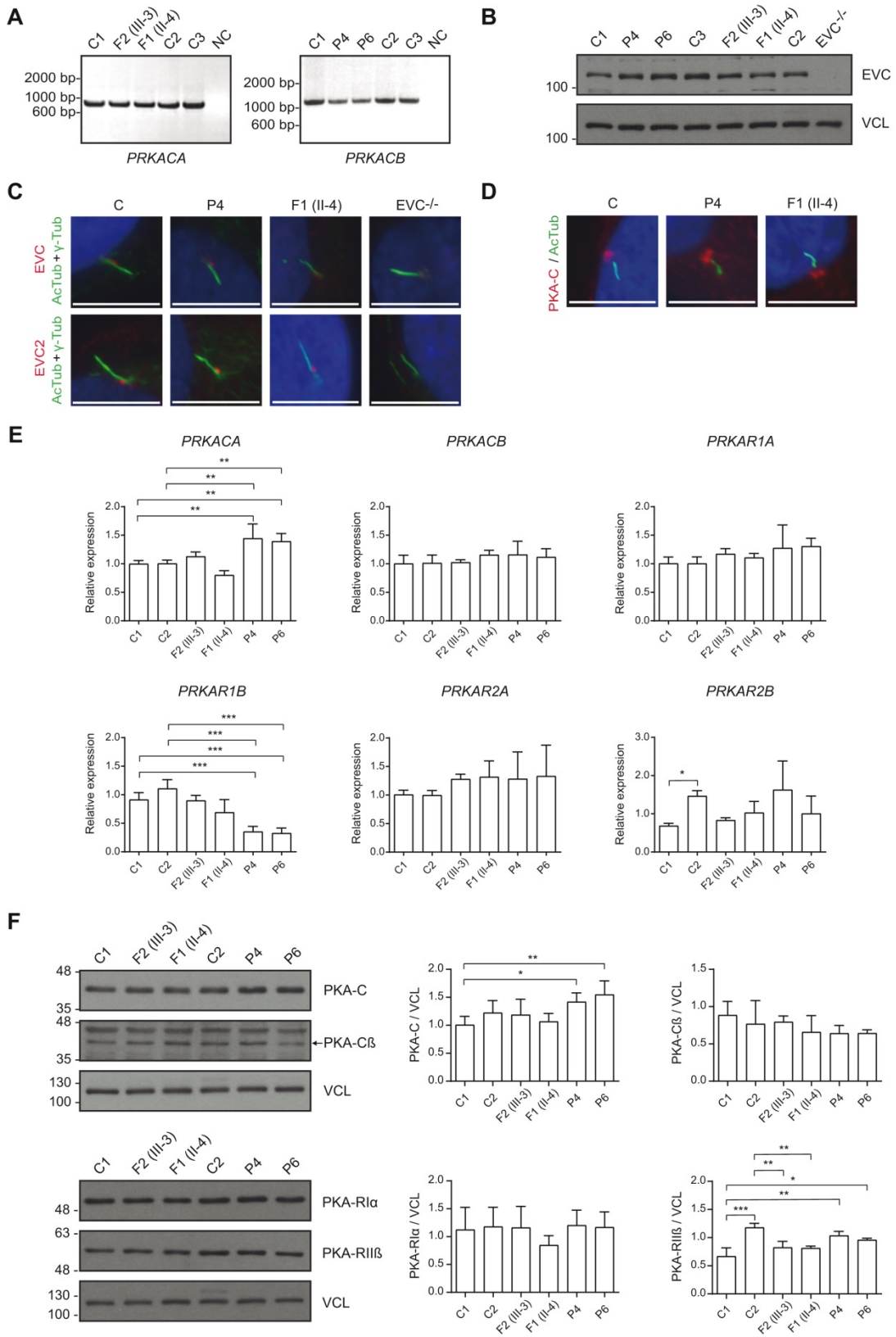


Figure S3. Expression analysis of EvC proteins and of PKA-C and PKA-R transcripts and proteins in primary fibroblasts. **A.)** RT-PCR demonstrating expression of both *PRKACA* and *PRKACB* transcripts in fibroblasts from controls (C1 and C2) and affected individuals (F2(III-3) and F1(II-4): C α -p.Gly137Arg; P4: C β -p.Gly235Arg; P6: C β -p.His88Arg [P: proband, F: family; family members are named as in Figure 1A]). NC is a negative control with no template. For each gene a forward primer upstream of the corresponding mutations and a reverse primer placed at the 3'-UTR were used (see methods for primer sequences). Direct sequencing of the amplified cDNA products confirmed the presence of the corresponding heterozygous missense mutations in samples from affected individuals indicating expression of both normal and mutant alleles. **B.)** Western Blot (WB) analysis of primary fibroblasts showing similar protein levels of EVC between normal controls (C) and affected subjects. Vinculin (VCL) was used as loading control. n=2. **C.)** Immunofluorescence images (shifted overlay) showing normal EVC and EVC2 localization at the base of primary cilia in fibroblasts from control (C) and affected individuals (P4 and F1(II-4)). EVC^{-/-} cells carrying loss of function mutations were used as negative control³, n=2. Red: EVC or EVC2; green: acetylated-tubulin (AcTub) and γ -tubulin (γ -Tub); blue (DAPI): nuclei. Scale bars: 10 μ m. **D.)** Immunofluorescence images showing PKA-C localization at the base of primary cilium of fibroblasts derived from control (C) and affected individuals (P4 and F1(II-4)), n=3. Red: PKA-C; green: acetylated-tubulin (AcTub); blue: nuclei. Scale bars: 10 μ m. **E.)** Relative mRNA quantification of PKA-C (*PRKACA*, *PRKACB*) and -R subunits (*PRKAR1A*, *PRKAR1B*, *PRKAR2A*, *PRKAR2B*) by qRT-PCR using TaqMan probes in fibroblasts from two independent normal controls (C1 and C2) and affected individuals (F2(III-3), F1(II-4), P4, P6). Values were normalized to *ACTB* and *GUSB* mRNA levels and represented as fold change of the mean value of C1 and C2. Graphs show means \pm SD, n = 4. * = P \leq 0.05, ** = P \leq 0.01, *** = P \leq 0.001 by one-way ANOVA followed by Tukey or Dunn's post-hoc test. **F.)** WB analysis of PKA-C, PKA-C β , PKA-R1 α and PKA-R11 β in fibroblasts from controls and affected individuals. The PKA-C antibody used (BD Transduction Laboratories (610980)) is raised against the C α -subunit, but due to amino acid conservation, we observed that it can recognize both C α and C β -subunits in extracts from cells transfected with individual FLAG-tagged C-subunits. Representative immunoblots are on the left and histograms show densitometric quantification of the different proteins referred to vinculin (VCL) that acted as loading control. Data are expressed as mean \pm SD, n=4 (PKA-C, PKA-C β); n=3 (PKA-R1 α , PKA-R11 β). * = P \leq 0.05, ** = P \leq 0.01, *** = P \leq 0.001 by one-way ANOVA followed by Tukey post-hoc test.

Figure S4

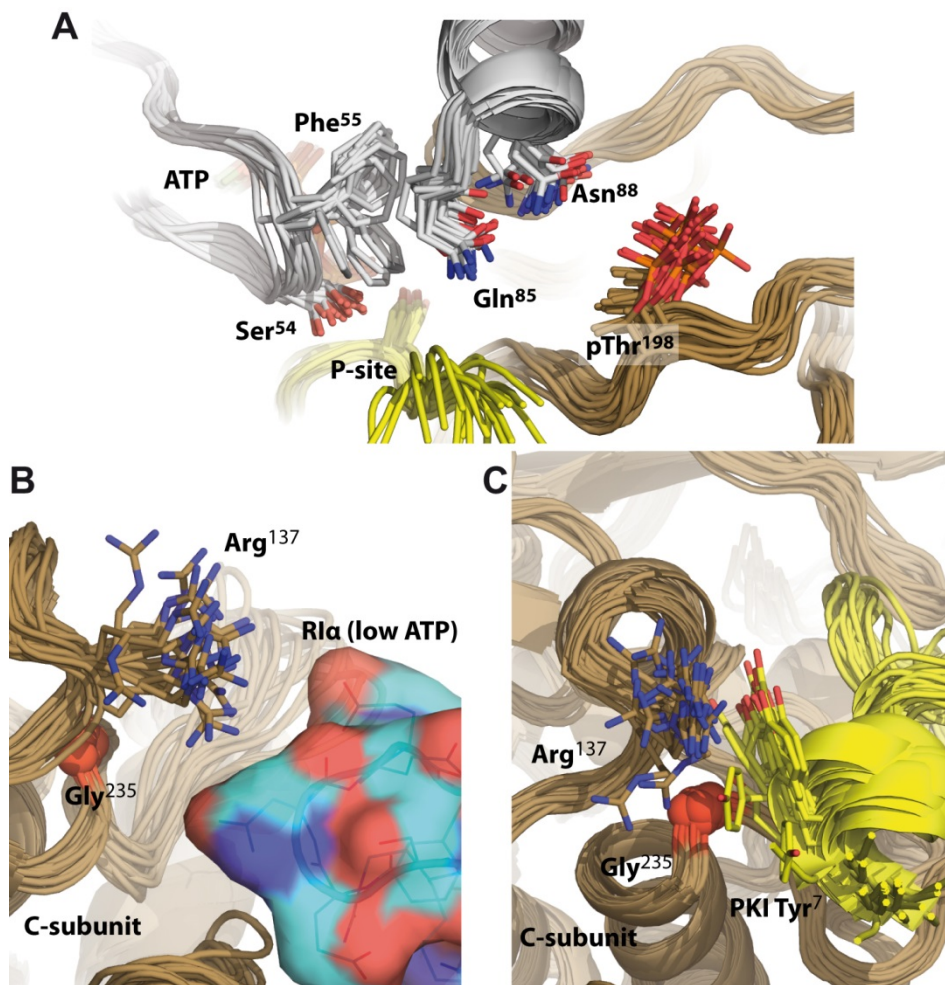


Figure S4. Effect of mutations on dynamics. A.) A change in G-loop dynamics compared to WT is observed in simulations for the C β -p.His88Asn mutation. This is similar to the C β -p.His88Arg mutation and likely leads to a change in synergistic ATP and substrate peptide binding. **B.)** The cAMP binding domain-B of R1 α docks into the pocket of the C-subunit perturbed by p.Gly137Arg and p.Gly235Arg mutants. This interaction is only observed in the low-ATP bound form of the R1 α holoenzyme⁴. **C.)** The tethering helix of PKI (5-24) also forms an interface with p.Gly137Arg and p.Gly235Arg.

Figure S5

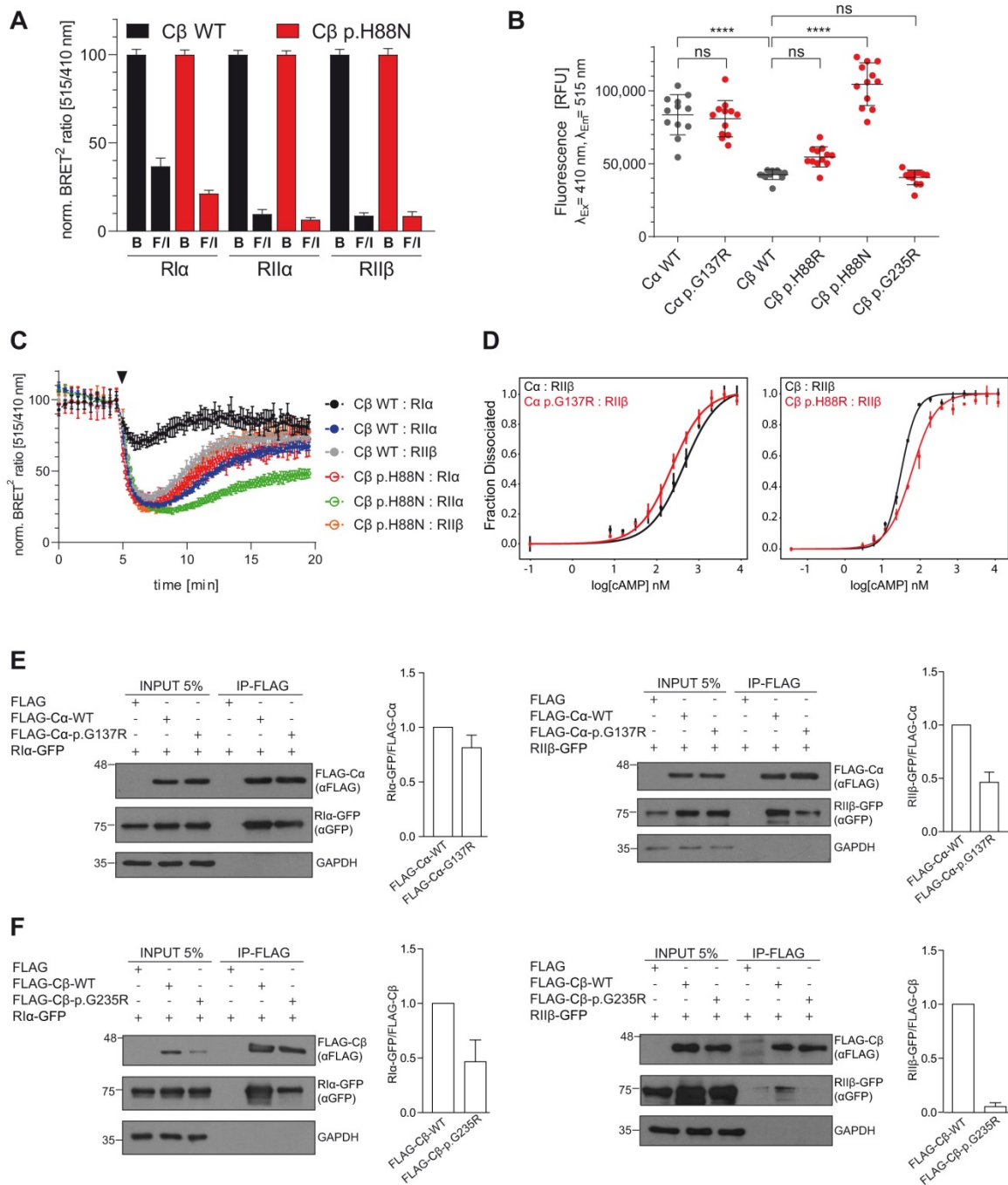


Figure S5. Functional characterization of PKA holoenzymes. A.) BRET² for Cβ-p.His88Asn (for conditions see figure legend 2E) demonstrating almost full dissociation upon F/I. Normalized data are shown as means (\pm SD) of 3 independent experiments with n=6 replicates each (total n=18). **B.)** Expression levels of GFP-tagged PKA-C-subunits in HEK293 cells: Ca-WT has a higher expression level compared to Cβ-WT while the mutant Cβ-p.His88Asn has a higher expression level than Cβ-WT. Statistics were done by one-way ANOVA followed by a Dunnett's Multiple Comparison (**** = $P \leq 0.0001$, ns = not significant) using n=12 replicates. **C.)** BRET² Kinetics for Cβ-p.His88Asn (for conditions

see Figure 2F) showing a reduced response after 100nM isoproterenol compared to C β -p.His88Arg. Data shown are means \pm SD of n=6 replicates showing one of 3 (2 for RII α) independent experiments. **D.)** FPA on RII β . The C α -p.Gly137Arg:RII β holoenzyme is easier to activate by cAMP compared to WT. The C β -p.His88Arg:RII β holoenzyme has an apparent decreased sensitivity to cAMP, however this is likely an artifact of the FPA experiment where the signal is dependent on fluorescent-PKI(5-24) peptide competing off the inhibitor segment of the holoenzyme regulatory subunit – the 10 fold decrease in PKI peptide affinity for C β -p.His88Arg increases the apparent activation constant (n=3). Graphs show mean \pm SD. **E-F.)** Co-immunoprecipitation (Co-IP) analysis. FLAG-immunoprecipitation from HEK293T co-transfected with the indicated constructs showing decreased interaction of C α -p.Gly137Arg and C β -p.Gly235Arg with regulatory subunits RI α or RII β with respect to the corresponding WT proteins. Plasmids included in each transfection are marked as +. GAPDH levels acted as loading control. Bar graphs show RI α -GFP/FLAG-C α or RII β -GFP/FLAG-C α ratio calculated by densitometry from the blots on the left. In each blot values were normalized to the value of the WT protein, n=3. Data are mean \pm SD.

Figure S6

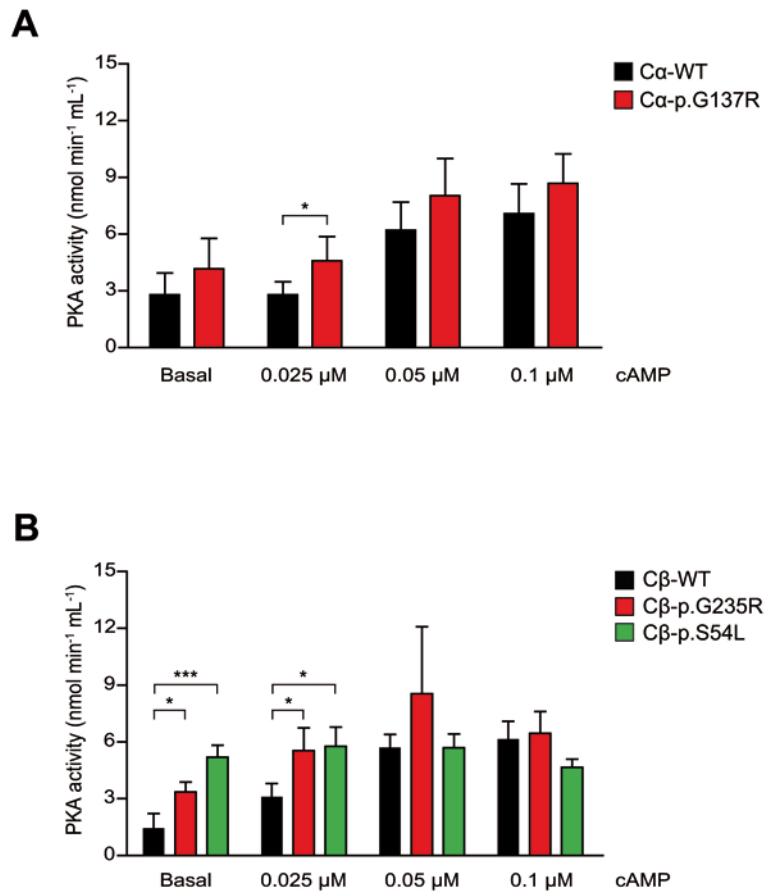


Figure S6. Effect of *PRKACA* and *PRKACB* mutations on PKA kinase activity. A-B.) PepTag assay using extracts from HEK293T co-transfected with FLAG-C and R1α-GFP subunits. This experiment revealed higher kinase activity of Cα-p.Gly137Arg compared to Cα-WT at 0.025 μM of cAMP (A). Cβ-p.Gly235Arg also shows higher kinase activity than Cβ-WT both at basal and after addition of 0.025 μM of cAMP. This is comparable with the previously reported activating PKA mutation, Cβ-p.Ser54Leu, which was included as control⁵ (B). Data represent the mean ± SD of four independent experiments. * = $P \leq 0.05$; *** = $P \leq 0.001$ by one-way ANOVA followed by Tukey post-hoc test.

Figure S7

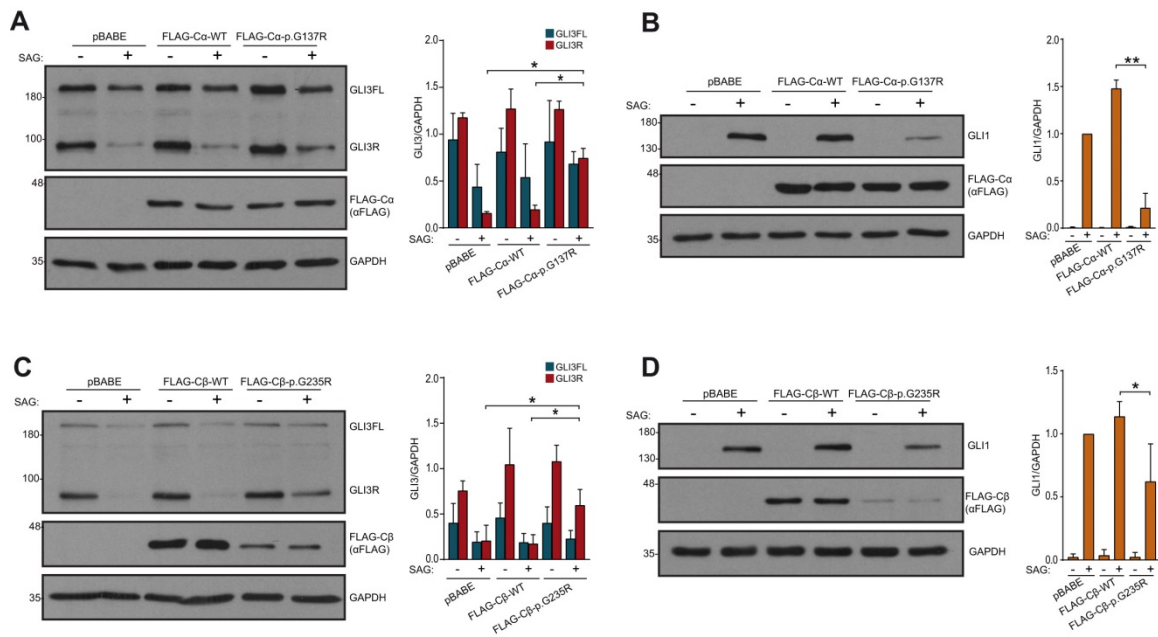


Figure S7. Impact of *PRKACA* and *PRKACB* mutations in Hh signaling evaluated in NIH 3T3 retrotransduced only with C-subunits. A-D.) Analysis of GLI3 and GLI1 protein levels in NIH 3T3 retrotransduced with human FLAG-Cα-WT or FLAG-Cα-p.Gly137Arg retroviral vectors (A-B), or alternatively, with FLAG-Cβ-WT or FLAG-Cβ-p.Gly235Arg retroviruses (C-D), exposed to SAG (+) or its vehicle DMSO (-). Expression levels of FLAG-C are shown in the underneath panels. After incubation with SAG, Cα-p.Gly137Arg and Cβ-p.Gly235Arg retrotransduced cells showed increased levels of GLI3R and reduced amount of GLI1 in comparison to cells retrotransduced with pBABE (empty vector) or with FLAG-Cα-WT or FLAG-Cβ-WT. Representative immunoblots are on the left and histograms represent densitometric quantification of the levels of GLI3R and GLI3FL referred to GAPDH (A and C) or GLI1/GAPDH levels normalized to the value of SAG-pBABE cells (B and D). Data are expressed as mean ± SD from two, (A-B) or three (C-D) independent retroviral infections. * = P < 0.05; ** = P < 0.01; Student's t-test.

Figure S8

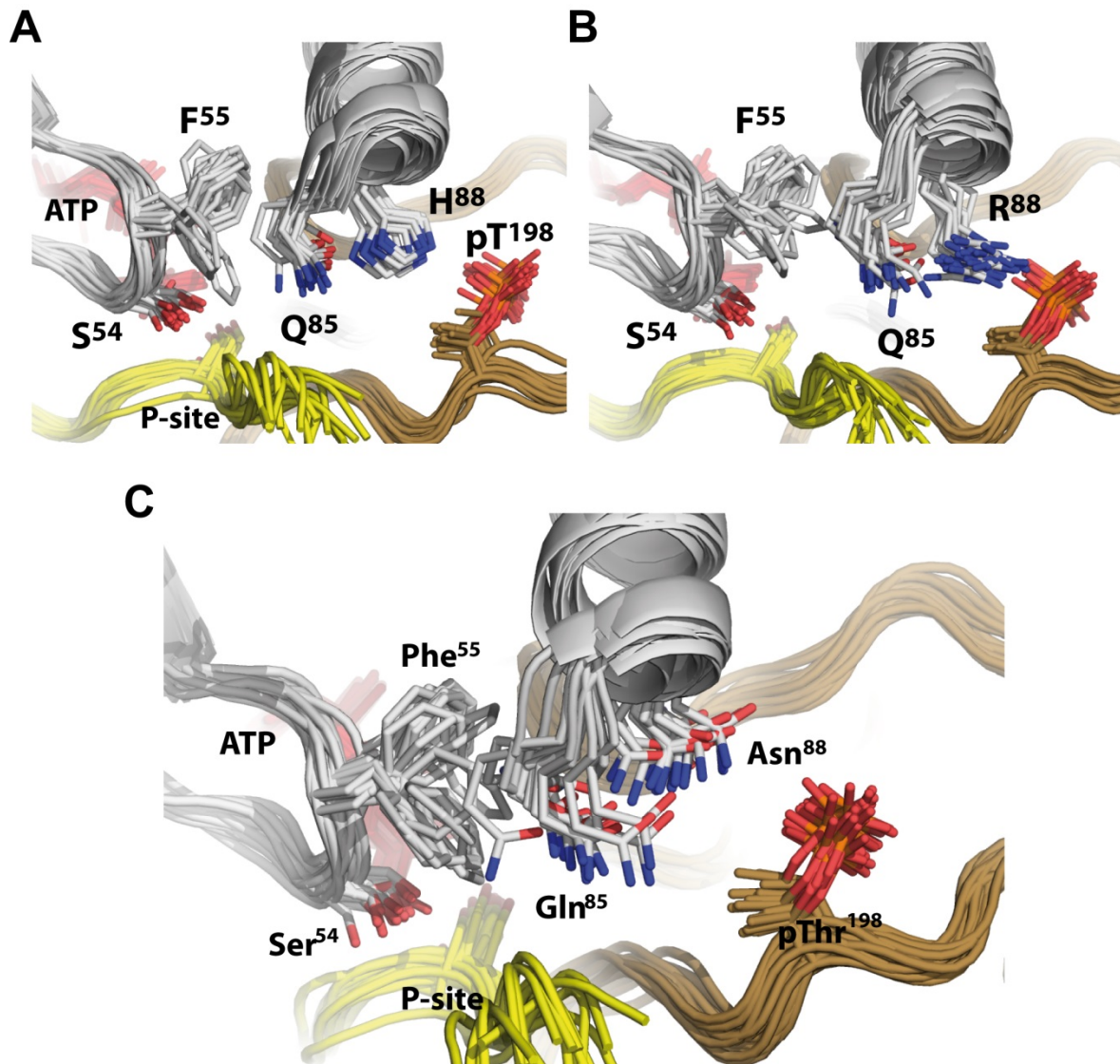


Figure S8. Molecular dynamics (MD) simulations of non-canonical C β 1 isoform sequence (BC035058). Images illustrate identical effects on dynamics due to disease mutation as MD simulations of canonical C β 1 sequence NM_002731 shown in Figure 2A-B and S4A. Panels A, B and C correspond to C β -WT, -p.His88Arg and -p.His88Asn, respectively.

Supplemental Tables

Table S1. Binding and activation constants for C β -p.His88Arg and C α -p.Gly137Arg

		C α -WT	C α -p.Gly137Arg	C β -WT	C β -p.His88Arg
C:ligand					
IP20	Kd	1.12 \pm 0.05 nM*	0.73 \pm 0.04 nM*	3.7 \pm 0.1 nM	37.1 \pm 1.8 nM
ATP	EC ₅₀	94.0 \pm 3.5 nM	54.4 \pm 2.5 nM	182.0 \pm 11.8 nM	6000 \pm 7000 nM
C2:R2 cAMP activation					
R1 α : C	EC ₅₀	8.15 \pm 0.22 nM	4.41 \pm 0.15 nM	24.2 \pm 1.4 nM	15.1 \pm 1.8 nM
	Hill	1.39 \pm 0.05	1.36 \pm 0.05	1.01 \pm 0.05	1.04 \pm 0.11
R1 β : C	EC ₅₀	440.8 \pm 47.5 nM	226.9 \pm 16.6 nM	31.3 \pm 1.0 nM	60.1 \pm 3.4 nM [†]
	Hill	1.07 \pm 0.11	1.11 \pm 0.08	2.11 \pm 0.12	1.36 \pm 0.09

Kd: dissociation constant. EC₅₀: apparent half maximal effective concentration. Hill: Hill coefficient.

*1nM detectable limit, [†] EC₅₀ is dominated by FAM-IP20 low affinity binding. Fitted values show the standard error of the mean (SEM).

Supplemental Methods

Genetic analysis

Peripheral blood genomic DNA was used in all genetic studies. Mutations in *EVC*-responsible genes *EVC* and *EVC2* were excluded in four individuals (P1-P4) by direct Sanger sequencing of all coding exons of both genes and MLPA analysis (MRC-Holland) (P1, P2, P4), or by means of a gene-targeted NGS clinical panel (P3). Trio (proband and both parents)-whole exome sequencing (WES) was performed in families 2, 4, 6 and 7 using standard DNA capture and variant filtering methodology. In family 5 only the affected child was analyzed by WES. In family 1, WES was conducted in the proband, one affected daughter (II-3 in Figure 1A) and her mother. WES was also performed in the affected fetus of family 2. In P3, *PRKACA* and *PRKACB* were screened by Sanger sequencing. In addition to standard WES, high-depth WES was carried out in P1 and the father of P2 to further confirm the mosaic state of the detected mutation.

Ensemble modeling by Molecular Dynamics

All complexes were prepared from the crystal structure of PKA in a closed ternary conformation bound with PKI (5-24) inhibitor peptide, ATP, and two Mn^{+2} ions (PDB code 3FJQ)⁶. The sequence was modified to match human *PRKACA* (NM_002730) or *PRKACB* (β 1 isoform BC035058 and NM_002731), Mn ions were changed to Mg, and Ser140, Thr198 and Ser339 were phosphorylated. N-terminal residues that were missing due to disorder in the original crystal structure were built based on the N-terminal structure of myristylated PKA (PDB code 1CMK)⁷, removing the myristyl moiety from the models. Mutations for C β -p.His88Arg/Asn and C α -p.Gly137Arg were generated from the wild-type models. The inhibitor peptide was mutated to the pseudo-substrate sequence PKS: TTYADFIASGRTGRRASIHD. The RII β inhibitory segment was taken from the RII β crystal structure (PDB code 3TNP)⁸, AGAFNAPVINRFTRRASVCAEAYNPD, and superposed onto the human PKA models. Five complexes, C β -p.His88Arg:PKS, C β -p.His88Asn:PKS, C β :PKS, C α -p.Gly137Arg:RII β , and C α :RII β were generated. Hydrogens and counter ions were added and the models were solvated in a cubic box of TIP4P-EW water⁹ and 150mM KCl with a 15 Å buffer in AMBERtools¹⁰. Parameters from the Bryce AMBER Parameter Database were used for ATP¹¹, phosphothreonine¹², and phosphoserine¹². Protonation states of histidines were optimized for neutral pH, specifically H88 was protonated. AMBER16¹⁰ was used for energy minimization, heating, and equilibration steps, using the GPU DPFP code for minimization and the GPU SPFP code for heating and equilibration.

Systems were minimized by 1000 steps of hydrogen-only minimization, 2000 steps of solvent minimization, 2000 steps of ligand minimization, 2000 steps of side-chain minimization, and 5000 steps of all-atom minimization. Systems were heated from 0 K to 300 K linearly over 250 ps with 2 fs time-steps and 5.0 kcal·mol⁻¹·Å position restraints on backbone atoms. Temperature was maintained by the Langevin thermostat. Constant pressure equilibration with a 10 Å non-bonded cut-off was performed with 300 ps of backbone restraints followed by 510 ps without restraints. A 10 Å cut-off for non-bonded interactions with particle mesh Ewald was used for a final 4 ns of equilibration. Production simulations were performed on GPU enabled AMBER16 for 1 ns. 20 independent minimization, equilibration, and production runs of each of the four complexes were performed. All atom RMSD was used to confirm equilibration of the system. The last frame of each trajectory was used as a representative model in the ensemble. The R1α (PDB code 6NO7)⁴ holoenzyme structure was superposed with the models to illustrate the effect of mutations on the holoenzyme complex.

Bioluminescence resonance energy transfer (BRET²) assays

HEK293 cells were seeded in a 96-well microplate (Nunc™ Delta Surface; Thermo Scientific) with a density of 2 x 10⁴ cells per well cultured in DMEM (Capricorn Scientific) supplemented with 10 % FCS (Capricorn Scientific). Cells were transiently cotransfected with GFP²-tagged PKA Cα-WT/Cβ1-WT or a mutant (Cα-p.Gly137Arg, Cβ1-p.His88Arg, Cβ1-p.His88Asn, Cβ1-p.Gly235Arg) and the respective Rluc8-tagged¹³ PKA regulatory subunit at a total of 0.05 µg DNA per construct using polyethyleneimine (25 kDa, Polysciences GmbH) as previously described¹⁴. The reporter proteins were expressed for 46-48 h at 37°C and 6 % CO₂. For endpoint measurements, cells were washed with Hanks' balanced salt solution (HBSS; Biowest) and incubated with 50 µM Forskolin (Sigma-Aldrich) and 100 µM IBMX (Sigma-Aldrich) or HBSS alone (untreated control) for 20 minutes prior to adding 5 µM Coelenterazine 400A, a luciferase substrate (DeepBlueC™; BIOTREND Chem)¹⁵. Emitted light was detected using a POLARstar Omega microplate reader (dual emission optics; BMG Labtech) with filters at wavelengths 410 ± 80 nm (Rluc8, donor) and 515 ± 30 nm (GFP², acceptor). Cells expressing Rluc8 alone were used as control for each experiment. By using GraphPad Prism 8.0 (GraphPad Software), the mean values (± standard deviation) were calculated from three independent measurements (each from 6 replicates), if not indicated otherwise. Data were normalized between the signal of unstimulated cells (buffer (B) only = 100%) and the Rluc8 control signal (0%). For kinetic measurements, transfected cells were washed with HBSS before the reaction was started upon the addition of 5 µM Coelenterazine 400A

with a total measuring time of 20 minutes. Different concentrations of isoproterenol (Sigma-Aldrich) were injected after 5 minutes at a final concentration of 100 nM in HBSS supplemented with 5 μ M Coelenterazine 400A. For application into the wells the reagent injector of the microplate reader was used. BRET² ratios were calculated from the 515 nm (GFP²-signal) to 410 nm (luciferase-signal) ratio. Data was analyzed with GraphPad Prism 8.0 by plotting the normalized BRET²-ratio against the time (kinetic measurements).

For quantification of expression level, cells were transiently transfected with the respective GFP²-tagged C-subunit (C α -WT, C α -p.Gly137Arg, C β 1-WT, C β 1-p.His88Arg, C β 1-p.His88Asn, C β 1-p.Gly235Arg) and treated as described for untreated controls in the endpoint BRET² measurements. Data point acquisition took place with a CLARIOstar microplate reader (BMG Labtech) at excitation and emission wavelength of 410 \pm 8 nm and 515 \pm 10 nm, respectively. Each well was scanned in a 10x10 scan matrix (5 mm diameter) with 8 flashes per scan point. Gain adjustment of fluorescence was set at 10% of the maximum fluorescence intensity (260,000 RFU, relative fluorescence units) against the Rluc8 control well (cells only transfected with Rluc8 without GFP²-tagged protein transfection). Data were analyzed with GraphPad Prism 8.0 by plotting obtained fluorescence intensity as scatter dot blot with mean \pm SD against the transfected constructs. For BRET² and the rest of experimental procedures NM_002730.4 (C α) and NM_002731.3 (C β 1) reference sequences were used unless otherwise specified.

Co-immunoprecipitation (Co-IP)

Mutant C α and C β 1 subunits were generated by directed mutagenesis using QuikChange II Site-Directed Mutagenesis Kit (Agilent Technologies) or amplified from fibroblast cDNA of affected individuals generated with superscript IV (Life Technologies). C- and R-subunits were cloned into pFLAG-CMV4 and pEGFP-N1, respectively. For transfections, HEK293T were cultured in growth medium (Dulbecco's modified Eagle's medium (DMEM) supplemented with 10% fetal bovine serum (FBS) and 1 X antibiotic-antimycotic (Gibco)) at 37°C and 5% (v/v) CO₂. Cells were seeded at a density of 2.5x10⁶ cells/P100 and co-transfected by the calcium phosphate method with a DNA mix containing 5 μ g of a FLAG-C β 1 plasmid and 5 μ g of a construct carrying R1 α -GFP or R11 β -GFP. In co-transfections using FLAG-C α subunits, 2 μ g of C- and 2 μ g of R-constructs were used. Cells were lysed 44 h after transfection in immunoprecipitation buffer 1X (Dynabeads Co-Immunoprecipitation Kit, Life technologies, 14321D) containing protease inhibitors and 150mM (R1 α Co-IP) or 300mM (R11 β Co-IP) of NaCl. Subsequently, 500 μ g (C β Co-IP) or 200 μ g (C α Co-IP) of protein extracts were incubated with 10 μ g of anti-FLAG M2

Magnetic beads (M8823, Sigma-Aldrich) and maintained 1 h in rotation at RT. Following three washes with TBS 1X, the beads were boiled in Laemmli sample buffer containing DTT (100 mM) for 5 min and processed for Western Blotting.

Western blot

Western blot (WB) analysis was performed as previously described³. Cell lysis was carried out in RIPA buffer (50 mM Tris-HCl pH 7.5, 150 mM NaCl, 2 mM EDTA, 1% NP40, 0.1% SDS, 0.5% Sodium deoxycholate) supplemented with protease and phosphatase inhibitors (Sigma, P8340, P0044 and P5726, 2.5 mM Na₃O₄V and 10 mM NaF). Primary antibodies: anti-mouse GLI1 (1:500; Cell Signaling, L42B10), anti-human/mouse GLI3 (0.4 µg/mL; R&D, AF3690), anti-α-Tubulin (1:80000; Sigma, T9026), anti-human EVC (1:1500; Sigma, HPA016046), anti-PKA-C (1:1000; BD Transduction Laboratories, 610980), anti-Cβ (1:1000, antisera SNO157)¹⁶, anti-R1α (1:1000, Cell Signaling, 5675), anti-R11β (1:1000, BD Transduction Laboratories, 610625), anti-Vinculin (1:2000; Santa Cruz sc-73614), anti-GAPDH (1:10000; Thermo Fisher, AM4300), anti-FLAG (1:2000 in Co-IPs, 1:500-retroviral infections; Sigma, F1804), anti-GFP (1:2000 in Co-IPs, 1:500-retroviral infections; Invitrogen, A6455). HRP-conjugated secondary antibodies were from Jackson ImmunoResearch. Blots were developed with ECL HRP substrate (Amersham) and exposed to X-Ray films. For protein quantification, films were scanned and densitometric analysis was conducted using ImageJ. GraphPad software 8.0 was used for statistical analysis.

Expression and Purification of Recombinant Proteins

The PKA catalytic subunit was expressed in *E. Coli* and purified as previously described⁴. Briefly, human isoforms of PKA-C were inserted into a pET15b expression system behind an N-terminal His-6-SUMO tag. The PRKACB (BC035058) sequence contained 3 amino acid differences compared to NM_002731: L163I, H159N, and H261N. These sequence differences likely have little impact on the interpretation since analysis is comparative to WT and the sequence difference is common within WT and disease mutant p.His88Arg. In addition, MD simulations of both canonical (Figure 2A-B and S4A) and non-canonical (Figure S8) Cβ sequences demonstrated identical effects on dynamics due to disease mutation. The PRKACA p.Gly137Arg and PRKACB p.His88Arg mutations were introduced into their respective WT isoform vectors using Phusion Site-Directed Mutagenesis PCR. After bacterial expression and Ni-Sepharose purification the His-SUMO tag was cleaved using His6-Ulp1 while dialyzing overnight at 277.15 K, producing native PKA-C. SUMO,

Ulp1, and uncleaved protein was removed by rebinding to Ni-Sepharose resin. A size exclusion Superdex-75 gel filtration column was used as a final purification step. Type I α and type II β R-subunits were recombinantly expressed and purified as previously described⁴. PKA tetrameric holoenzymes were pre-formed via incubation with R-subunit and C-subunit at a 1:1.3 (R:C) molar ratio and purified over a Superdex-200 gel filtration column to remove excess C-subunit. Type I α holoenzyme, at $\sim 1 \mu\text{M}$, was formed and purified in the presence of 5 mM MgCl₂ and 200 μM ATP.

LiReC Fluorescence Polarization Assay (FPA)

The LiReC assay was performed as described previously¹⁷. In brief, activation experiments were performed using two-fold serial dilutions in assay buffer: 20 mM HEPES pH 7.0, 75 mM KCl, 0.005% Triton-X100, 10 mM MgCl₂. Either 12 or 14 concentrations were tested in triplicate. Fluorescence polarization signal was measured 15 min after addition of titrant via GENios Plate-reader (Tecan). The stability of holoenzyme was characterized by titration of 1.95 nM - 8 μM cAMP into 12nM of R:C holoenzyme complex, 2-3 nM FAM-IP20, 1 mM ATP (RI α) or 1 mM AMP-PNP (RII β). ATP concentration-dependent binding of IP20 was measured via titration of ATP (14.5 nM to 15 μM) into 2 nM FAM-IP20 and 5 nM of purified C-subunit. The binding affinity of the inhibitor peptide to C-subunit was assessed in the presence of saturating ATP via titration of C-subunit (0.39 nM to 400 nM) in 2nM FAM-IP20 and 1 mM ATP.

PKA activity assay

HEK293T were seeded at density of 3×10^6 cells/P100 in growth medium and allowed to grow for 24 h before being transfected with the calcium phosphate method. DNA ratios of 1:8 FLAG-C α :RI α -GFP and 1:1 FLAG-C β 1:RI α -GFP were used to facilitate association between C- and R-subunits as previously reported¹⁸. Twenty-four h after transfection cells were trypsinized, washed in cold PBS, and resuspended in 300 μL of buffer containing 5 mM Tris-HCl (pH 7.4), 2 mM EDTA. Cells were homogenized using an Ultraturrax homogenizer for 20 s on ice and centrifuged at 16000 g for 30 min at 4°C. To measure PKA catalytic activity in cell homogenates the PepTag nonradioactive cAMP-dependent protein kinase assay (Promega) that uses a fluorescent Kemptide as substrate was used following the manufacturer's instructions. Samples were tested in the absence or presence of increasing concentrations of cAMP (0.025 μM , 0.05 μM and 0.1 μM) and the PKA kinase activity was quantified by spectrophotometry after separation of the phosphorylated peptide in an agarose gel. PKA kinase activity was calculated as indicated

in the protocol provided by the manufacturer and is expressed in nanomoles of phosphate transferred to PepTag peptide per $\text{min}^{-1} \text{mL}^{-1}$ in the reaction. GraphPad software 8.0 was used for statistical analysis.

Retroviral infection

HEK293T cells seeded in P100 plates (3×10^6 /P100) were co-transfected using the calcium phosphate method with 10 μg of the packaging plasmid pCL-Eco and 10 μg of the pBABE retroviral vector either empty, or carrying the human sequence of a specific N-terminal FLAG-tagged C-subunit, or a R1 α -GFP fusion protein. Supernatants were collected 44, 52 and 70 h post-transfection and filtered through a 0.45 μm syringe filter (Millipore). Supernatants were diluted 0.5:0.5:1 of pBABE-FLAG-C: pBABE-R1 α -GFP: growth medium with polybrene, and then applied to NIH 3T3 cells seeded at 3×10^5 /P60. In total, three consecutive infections were performed, one after each supernatant collection using polybrene at 8 $\mu\text{g}/\text{mL}$, 4 $\mu\text{g}/\text{mL}$ and 8 $\mu\text{g}/\text{mL}$, respectively. Cells were left to recover for 24 h after the last infection, and subsequently were subjected to puromycin (2 $\mu\text{g}/\text{mL}$) selection for 72 h. In experiments in which R1 α was not included, NIH 3T3 were infected as indicated above with a ratio 1:1 of supernatant containing FLAG-tagged-C-subunit retroviruses and growth medium. Puromycin resistant NIH 3T3 cells were plated at a density of 1×10^6 cells/P100 in growth medium and 24 h later transferred to low serum medium (DMEM with 0.5% FBS and 1 X antibiotic-antimycotic (Gibco)) supplemented with SAG (100nM, Calbiochem) or its vehicle DMSO (Sigma-Aldrich) and maintained for another 24 h before being analyzed by WB.

RT-PCR and qRT-PCR

Total RNA was purified from primary fibroblasts with TriReagent solution (Sigma-Aldrich) according to manufacturer's instructions and used to synthesize cDNA with SuperScript™ IV First-Strand Synthesis System kit (Invitrogen) and random primers. Fibroblast cDNA was subsequently used as template to amplify a cDNA fragment of *PRKACA* and other of *PRKACB* with GoTaq DNA polymerase (Promega). Forward primers were located upstream of the identified *PRKACA* and *PRKACB* mutations and the reverse primers were from the 3'-UTR of each gene (*PRKACA*-FW: 5'-ATGCCATGAAGATCCTCGAC-3'; *PRKACA*-RV: 5'-ACAGGCATGCCCTAAACT-3'; *PRKACB*-FW: 5'-AGGTGGAGAGCGTGAAAGAG-3'; *PRKACB*-RV: 5'-GCTTCAACAAGGACGGTCTC-3'). Amplified products were directly sequenced to confirm the presence of mutant alleles in the heterozygous state in mRNA from affected individuals. For qRT-PCR analysis, total

RNA from fibroblasts was isolated with TriReagent solution and retrotranscribed using the High Capacity cDNA Reverse Transcription Kit (Applied Biosystems). qRT-PCR experiments were performed in a 7900HT Fast Real-Time PCR System (Applied Biosystems) using TaqMan real-time PCR gene expression assays (Applied Biosystems/ Thermo Fisher Scientific). For each line of fibroblasts, RNA from four independent extractions was used and every sample was run in triplicates. Transcript levels were normalized against the geometric mean of two housekeeping genes (*ACTB* and *GUSB*). Fold differences in gene expression were calculated by the $2^{-\Delta\Delta Ct}$ method using the mean of the two normal control cultures included in the analysis as the calibrator sample. Taqman assays were as follows: *ACTB* (Hs99999903_m1), *GUSB* (Hs99999908_m1), *PRKACA* (Hs00427274_m1), *PRKACB* (Hs01086757_m1), *PRKAR1A* (Hs00267597_m1), *PRKAR1B* (Hs00406762_m1), *PRKAR2A* (Hs00177760_m1), *PRKAR2B* (Hs00176966_m1).

Immunofluorescence

Primary fibroblasts were plated onto cover slips in 24-multiwell plates (1×10^5 /well) in growth medium. After 24 h, the media was replaced to low serum medium for another 24 h. Cells were fixed, permeabilized and incubated with primary and secondary antibodies as previously described¹⁹. Primary antibodies: acetylated tubulin (Sigma (T7451), 1:2000), γ -tubulin (Sigma (T5326), 1:2000), EVC (Sigma (HPA016046), 1:350), EVC2 (Abcam (ab198930) 1:500) and PKA-C (BD Transduction Laboratories (610980) 1:500). Secondary antibodies (1:1000), DAPI (1:2000) and Prolong Diamond antifade mounting medium were from Molecular Probes.

Supplemental References

1. Kim, S.E., Lei, Y., Hwang, S.H., Wlodarczyk, B.J., Mukhopadhyay, S., Shaw, G.M., Ross, M.E., and Finnell, R.H. (2019). Dominant negative GPR161 rare variants are risk factors of human spina bifida. *Hum Mol Genet* 28, 200-208.
2. Karaca, E., Buyukkaya, R., Pehlivan, D., Charng, W.L., Yaykasli, K.O., Bayram, Y., Gambin, T., Withers, M., Atik, M.M., Arslanoglu, I., et al. (2015). Whole-exome sequencing identifies homozygous GPR161 mutation in a family with pituitary stalk interruption syndrome. *J Clin Endocrinol Metab* 100, E140-147.
3. Caparros-Martin, J.A., Valencia, M., Reytor, E., Pacheco, M., Fernandez, M., Perez-Aytes, A., Gean, E., Lapunzina, P., Peters, H., Goodship, J.A., et al. (2013). The ciliary Evc/Evc2 complex interacts with Smo and controls Hedgehog pathway activity in chondrocytes by regulating Sufu/Gli3 dissociation and Gli3 trafficking in primary cilia. *Hum Mol Genet* 22, 124-139.
4. Lu, T.W., Wu, J., Aoto, P.C., Weng, J.H., Ahuja, L.G., Sun, N., Cheng, C.Y., Zhang, P., and Taylor, S.S. (2019). Two PKA R1 α holoenzyme states define ATP as an isoform-specific orthosteric inhibitor that competes with the allosteric activator, cAMP. *Proc Natl Acad Sci U S A* 116, 16347-16356.
5. Espiard, S., Knape, M.J., Bathon, K., Assie, G., Rizk-Rabin, M., Faillot, S., Luscap-Rondof, W., Abid, D., Guignat, L., Calebiro, D., et al. (2018). Activating PRKACB somatic mutation in cortisol-producing adenomas. *JCI Insight* 3, e98296. <https://doi.org/10.1172/jci.insight.98296>.
6. Thompson, E.E., Kornev, A.P., Kannan, N., Kim, C., Ten Eyck, L.F., and Taylor, S.S. (2009). Comparative surface geometry of the protein kinase family. *Protein Sci* 18, 2016-2026.
7. Zheng, J., Knighton, D.R., Xuong, N.H., Taylor, S.S., Sowadski, J.M., and Ten Eyck, L.F. (1993). Crystal structures of the myristylated catalytic subunit of cAMP-dependent protein kinase reveal open and closed conformations. *Protein Sci* 2, 1559-1573.
8. Zhang, P., Smith-Nguyen, E.V., Keshwani, M.M., Deal, M.S., Kornev, A.P., and Taylor, S.S. (2012). Structure and allostery of the PKA R11 β tetrameric holoenzyme. *Science* 335, 712-716.
9. Horn, H.W., Swope, W.C., Pitera, J.W., Madura, J.D., Dick, T.J., Hura, G.L., and Head-Gordon, T. (2004). Development of an improved four-site water model for biomolecular simulations: TIP4P-Ew. *J Chem Phys* 120, 9665-9678.

10. Case DA, B.R., Botello-Smith W, Cerutti DS, Cheatham TE, Darden TA, Duke RE, Giese TJ, Gohlke H, Goetz AW, Homeyer N, Izadi S, Janowski P, Kaus J, Kovalenko A, Lee TS, LeGrand S, Li P, Lin C, Luchko T, Luo R, Madej B, Mermelstein D, Merz KM, Monard G, Nguyen H, Nguyen HT, Omelyan I, Onufriev A, Roe DR, Roitberg A, Sagui C, Simmerling CL, Swails J, Walker RC, Wang J, Wolf RM, Wu X, Xiao L, York DM, Kollman PA. (2016). Amber (University of California, San Francisco).
11. Meagher, K.L., Redman, L.T., and Carlson, H.A. (2003). Development of polyphosphate parameters for use with the AMBER force field. *J Comput Chem* 24, 1016-1025.
12. Homeyer, N., Horn, A.H., Lanig, H., and Sticht, H. (2006). AMBER force-field parameters for phosphorylated amino acids in different protonation states: phosphoserine, phosphothreonine, phosphotyrosine, and phosphohistidine. *J Mol Model* 12, 281-289.
13. Loening, A.M., Fenn, T.D., Wu, A.M., and Gambhir, S.S. (2006). Consensus guided mutagenesis of Renilla luciferase yields enhanced stability and light output. *Protein Eng Des Sel* 19, 391-400.
14. Chepurny, O.G., Bertinetti, D., Diskar, M., Leech, C.A., Afshari, P., Tsalkova, T., Cheng, X., Schwede, F., Genieser, H.G., Herberg, F.W., et al. (2013). Stimulation of proglucagon gene expression by human GPR119 in enteroendocrine L-cell line GLUTag. *Mol Endocrinol* 27, 1267-1282.
15. Prinz, A., Diskar, M., and Herberg, F.W. (2006). Application of bioluminescence resonance energy transfer (BRET) for biomolecular interaction studies. *Chembiochem* 7, 1007-1012.
16. Orstavik, S., Funderud, A., Hafte, T.T., Eikvar, S., Jahnsen, T., and Skalhegg, B.S. (2005). Identification and characterization of novel PKA holoenzymes in human T lymphocytes. *FEBS J* 272, 1559-1567.
17. Saldanha, S.A., Kaler, G., Cottam, H.B., Abagyan, R., and Taylor, S.S. (2006). Assay principle for modulators of protein-protein interactions and its application to non-ATP-competitive ligands targeting protein kinase A. *Anal Chem* 78, 8265-8272.
18. Bathon, K., Weigand, I., Vanselow, J.T., Ronchi, C.L., Sbiera, S., Schlosser, A., Fassnacht, M., and Calebiro, D. (2019). Alterations in Protein Kinase A Substrate Specificity as a Potential Cause of Cushing Syndrome. *Endocrinology* 160, 447-459.
19. Palencia-Campos, A., Ullah, A., Nevado, J., Yildirim, R., Unal, E., Ciorraga, M., Barruz, P., Chico, L., Picci-Sparascio, F., Guida, V., et al. (2017). GLI1 inactivation is

associated with developmental phenotypes overlapping with Ellis-van Creveld syndrome.
Hum Mol Genet 26, 4556-4571.